

Chapter 2

Black Hole Solutions

In 4-dimensional general relativity and in the absence of exotic fields, black holes are completely described by three parameters: the mass M , the spin angular momentum J , and the electric charge Q . This is the conclusion of the no-hair theorem, which holds under specific assumptions. Violations of the no-hair theorem are possible. For instance, hairy black holes naturally emerge in the presence of non-Abelian gauge fields or of fields non-minimally coupled to gravity.

Starting from the Oppenheimer-Snyder model, which describes the gravitational collapse of a homogeneous ball of dust, we know how the complete collapse of a body forms a black hole with a central spacetime singularity. In extensions of general relativity, the picture of the collapse of a massive body may be somewhat different. It is possible that, strictly speaking, black holes cannot form, but only temporary apparent horizons can be created. The latter can however be interpreted as event horizons if the observation time is much shorter than the lifetime of the apparent horizon.

2.1 Definition of Black Hole

Roughly speaking, a black hole is a region of the spacetime in which gravity is so strong that it is impossible to escape or send information to the exterior region. A more technical definition is the following:

A *black hole* in an asymptotically flat spacetime \mathcal{M} is the set of events that do not belong to the causal past of the future null infinity $J^-(\mathcal{I}^+)$, namely

$$\mathcal{B} = \mathcal{M} - J^-(\mathcal{I}^+) \neq \emptyset. \quad (2.1)$$

The *event horizon* is the boundary of the region \mathcal{B} .

This definition of black hole uses the concepts developed by Penrose for studying causality and asymptotic properties of asymptotically flat spacetimes [49]. See also [42]. \mathcal{I}^+ indicates the future null infinity,¹ namely the region toward which outgoing null lines extend. Heuristically, in spherical-like coordinates, it is the region $t + r \rightarrow \infty$ at finite $t - r$. $J^-(\mathcal{P})$ is called the causal past of the region \mathcal{P} and is the set of all events that causally precede \mathcal{P} ; that is, there exists at least one smooth future-directed time-like curve extending from any element in $J^-(\mathcal{P})$ to \mathcal{P} . All future-directed curves (either time-like or null) starting from the region \mathcal{B} fail to reach null infinity \mathcal{I}^+ . A black hole is thus an actual one-way membrane: if something crosses the event horizon it can no longer send any signal to the exterior region.

The event horizon is a global property of an entire spacetime and it can be only determined if we know the whole spacetime, including the faraway future. It has thus no direct observational implications and, for this reason, it is often not a very useful concept in many studies. The apparent horizon is instead a local property of the spacetime and is slicing-dependent. Here we do not discuss all the details, which can be found, for instance, in [7, 42, 50, 60].

Let us consider a $3 + 1$ foliation of the spacetime. A *trapped surface* is a smooth closed 2-dimensional surface in a 3-dimensional space-like slice such that all null geodesics emanating from this surface are pointing inwards. The *trapped region* is the union of all the trapped surfaces of the slice. The *apparent horizon* is the outer boundary of the trapped region. Figure 2.1 shows a simple sketch illustrating these concepts. Outward-pointing light rays behind an apparent horizon thus move inwards and therefore they cannot cross the apparent horizon. In the case of an event horizon, the light rays may initially move outwards and then inwards at some later time. Under certain conditions, the existence of an apparent horizon implies that the slice contains an event horizon; however, the converse may not be true [61].

As it will be discussed in Sect. 2.5, it is possible that black holes cannot form in the Universe, but only apparent horizons can be created. Nevertheless, human observations may be completely unable to check the actual nature of the horizon of astrophysical black holes because any real observation only lasts for a finite time, which may be much shorter than the timescale necessary to distinguish the two scenarios.

An event horizon is a null surface in spacetime. Let us introduce a scalar function f such that at the event horizon $f = 0$. The normal to the event horizon is $n^\nu = \partial^\nu f$ and is a null vector. The condition for the surface $f = 0$ to be null is [12, 55]

$$g^{\mu\nu} (\partial_\mu f) (\partial_\nu f) = 0, \quad (2.2)$$

where $g_{\mu\nu}$ is the metric of the spacetime. In general, one can find the event horizon of a spacetime by integrating null geodesics backwards in time, see [12, 55] for the

¹The symbol \mathcal{I} is usually pronounced “scri”.

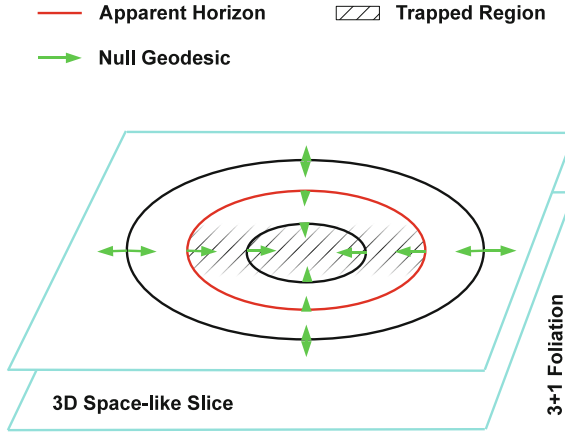


Fig. 2.1 Sketch of a 3-dimensional space-like slice with a trapped region (hatched area). Inside the trapped region, there are trapped surfaces. The outer boundary of the trapped region is the apparent horizon (*red closed curve*). The *green arrows* represent null geodesics. All the null geodesics emanating from the surfaces inside the trapped region move inwards. In the case of the surface outside the trapped region (*black closed curve* outside the hatched area), we see that the arrows can point either outwards or inwards. See the text for more details

details. In the case of a stationary and axisymmetric spacetime,² the procedure can significantly simplify. In a coordinate system adapted to the two Killing isometries (stationarity and axisymmetry), and such that f is also compatible with the Killing isometries, Eq. (2.2) reduces to

$$g^{rr} (\partial_r f)^2 + 2g^{r\theta} (\partial_r f) (\partial_\theta f) + g^{\theta\theta} (\partial_\theta f)^2 = 0 \quad (2.3)$$

in spherical-like coordinates (t, r, θ, ϕ) . The surface must be closed and non-singular (namely geodesically complete) in order to be an event horizon and not just a null surface.

If we assume that there is a unique horizon radius for any angle θ (Strahlkörper assumption), we can write f as $f = r - H(\theta)$, where $H(\theta)$ is a function of θ only and the event horizon is $r_H = H(\theta)$; see [12, 55] for the details and the limitations of the Strahlkörper assumption. The problem is thus reduced to finding the solution of the differential equation

$$g^{rr} + 2g^{r\theta} \left(\frac{dH}{d\theta} \right) + g^{\theta\theta} \left(\frac{dH}{d\theta} \right)^2 = 0. \quad (2.4)$$

²A space-time is *stationary* if it posses a time-like Killing vector field, and is *static* if it posses a hypersurface-orthogonal time-like Killing vector field. It is always possible to choose coordinates in which the time-like Killing vector field is ∂_t . In this case, in a stationary spacetime the metric is invariant under translations in t , namely the metric coefficients are independent of t . In a static spacetime, the time-like Killing vector is orthogonal to the hypersurfaces of constant t , which implies $g_{0i} = 0$.

Reference [30] argues that the event horizon equation $g^{rr} = 0$ (valid, for instance, in the Kerr spacetime in Boyer–Lindquist coordinates) would hold whenever the surfaces $r = \text{const.}$ have a well-defined causal structure, in the sense that any surface $r = \text{const.}$ must be null, space-like, or time-like. In such a case, the surface $r = H$ would be null and would correspond to the event horizon, the surfaces $r = \text{const.}$ at larger radii would be all space-like, and the surfaces $r = \text{const.}$ at smaller radii would be all time-like.

A *Killing horizon* is a null hypersurface on which there is a null Killing vector field. In a stationary and axisymmetric spacetime and employing a coordinate system adapted to the two Killing isometries, the Killing horizon is given by the largest root of

$$g_{tt}g_{\phi\phi} - g_{t\phi}^2 = 0. \quad (2.5)$$

In general relativity, the Hawking rigidity theorem shows that the event and the Killing horizons coincide [22], so Eqs. (2.4) and (2.5) provide the same result. In alternative theories of gravity, this is at least not guaranteed [30].

In general relativity, the event horizon must have $S^2 \times \mathbf{R}$ topology, and even this property is regulated by certain theorems [22, 29]. For instance, toroidal horizons can form, but they can only exist for a short time, in agreement with these theorems [27].

2.2 Black Holes in General Relativity

2.2.1 Schwarzschild Solution

In general relativity, the simplest black hole metric is the *Schwarzschild solution*, which describes the spacetime of a non-rotating uncharged black hole in a vacuum and asymptotically flat spacetime. In the Schwarzschild coordinates (t, r, θ, ϕ) , the line element is

$$ds^2 = -\left(1 - \frac{2M}{r}\right)dt^2 + \left(1 - \frac{2M}{r}\right)^{-1}dr^2 + r^2d\theta^2 + r^2\sin^2\theta d\phi^2, \quad (2.6)$$

where M is the mass of the black hole. The Schwarzschild metric is relatively straightforward to find and its derivation is presented in many textbooks.

As a consequence of Birkhoff's theorem, the Schwarzschild metric is the only spherically symmetric vacuum solution of the Einstein equations. This means it describes the exterior region of any spherically symmetric body, independently of its interior, which may also change in time (but maintaining its spherical symmetry).

The line element in Eq. (2.6) is singular at the surface $r = 2M$, in the sense that g_{tt} vanishes and g_{rr} diverges. This is the event horizon, as it can be seen from the procedure explained in the previous section. Here $H = 2M$ and is independent of θ .

The singularity is due to the choice of the coordinates, but the spacetime is regular there. For instance, the Kretschmann scalar \mathcal{K} is

$$\mathcal{K} = R^{\mu\nu\rho\sigma} R_{\mu\nu\rho\sigma} = \frac{48M^2}{r^6}. \quad (2.7)$$

The Kretschmann scalar only diverges at $r = 0$, which is the real singularity of the spacetime, both in the sense of curvature singularity (curvature invariants diverge) and in the sense that the spacetime is geodesically incomplete (any geodesic reaching $r = 0$ stops there).

The singularity at the event horizon can be removed by a change of coordinates. For instance, the Lemaitre coordinates (T, R, θ, ϕ) are related to the Schwarzschild coordinates by

$$\begin{aligned} dT &= dt + \left(\frac{2M}{r}\right)^{1/2} \left(1 - \frac{2M}{r}\right)^{-1} dr, \\ dR &= dt + \left(\frac{r}{2M}\right)^{1/2} \left(1 - \frac{2M}{r}\right)^{-1} dr, \end{aligned} \quad (2.8)$$

and the line element of the Schwarzschild solution becomes

$$ds^2 = -dT^2 + \frac{2M}{r} dR^2 + r^2 d\theta^2 + r^2 \sin^2 \theta d\phi^2, \quad (2.9)$$

where

$$r = (2M)^{1/3} \left[\frac{3}{2} (R - T) \right]^{2/3}. \quad (2.10)$$

The metric is now regular at the event horizon $r = 2M$, corresponding to the points $4M = 3(R - T)$, and it is still singular at $r = 0$, $R = T$, which is indeed the true singularity in this spacetime.

Other common coordinates to write the Schwarzschild solution are the Kruskal–Szekeres coordinates, the Eddington–Finkelstein coordinates, and the Gullstrand–Painlevé coordinates. The Kruskal–Szekeres coordinates are employed to write the maximal analytic extension of the Schwarzschild solution. In this case, the line element reads

$$ds^2 = -\frac{32M^3}{r} e^{-r/(2M)} dV dU + r^2 d\theta^2 + r^2 \sin^2 \theta d\phi^2, \quad (2.11)$$

where $U = \tau - \rho$ and $V = \tau + \rho$ are light-cone coordinates and

$$\begin{aligned}\tau &= \begin{cases} \left(\frac{r}{2M} - 1\right)^{1/2} e^{r/(4M)} \sinh\left(\frac{t}{4M}\right) & \text{if } r > 2M, \\ \left(1 - \frac{r}{2M}\right)^{1/2} e^{r/(4M)} \cosh\left(\frac{t}{4M}\right) & \text{if } 0 < r < 2M. \end{cases} \\ \rho &= \begin{cases} \left(\frac{r}{2M} - 1\right)^{1/2} e^{r/(4M)} \cosh\left(\frac{t}{4M}\right) & \text{if } r > 2M, \\ \left(1 - \frac{r}{2M}\right)^{1/2} e^{r/(4M)} \sinh\left(\frac{t}{4M}\right) & \text{if } 0 < r < 2M. \end{cases}\end{aligned}\quad (2.12)$$

As briefly discussed in Sect. 2.6, the maximal extension of the Schwarzschild solution includes also a white hole and a parallel universe, which are not present in the Schwarzschild spacetime in Schwarzschild coordinates.

2.2.2 Reissner–Nordström Solution

If a non-rotating black hole has a non-vanishing electric charge, the metric is described by the *Reissner–Nordström solution*. As a useful recipe to remember, the Reissner–Nordström line element can be obtained from the Schwarzschild one in Eq. (2.6) with the substitution $M \rightarrow M - Q^2/(2r)$, where Q is the electric charge of the black hole. The result is³

$$ds^2 = -\left(1 - \frac{2M}{r} + \frac{Q^2}{r^2}\right) dt^2 + \left(1 - \frac{2M}{r} + \frac{Q^2}{r^2}\right)^{-1} dr^2 + r^2 d\theta^2 + r^2 \sin^2 \theta d\phi^2. \quad (2.14)$$

The solution of $g^{rr} = 0$ is

$$r_{\pm} = M \pm \sqrt{M^2 - Q^2}, \quad (2.15)$$

where the larger root, r_+ , is the event horizon, while the smaller root, r_- , is the inner horizon. The latter is a Cauchy horizon and is unstable [13, 51]. The horizons only exist for $|Q| \leq M$. For $|Q| > M$, there is no horizon, the singularity at $r = 0$ is naked, and the Reissner–Nordström solution describes the spacetime of a naked singularity rather than that of a black hole.

³In international system units, the line element reads (reintroducing also G_N and c)

$$ds^2 = -\left(1 - \frac{2G_N M}{c^2 r} + \frac{G_N Q^2}{4\pi \epsilon_0 c^4 r^2}\right) dt^2 + \left(1 - \frac{2G_N M}{c^2 r} + \frac{G_N Q^2}{4\pi \epsilon_0 c^4 r^2}\right)^{-1} dr^2 + r^2 d\theta^2 + r^2 \sin^2 \theta d\phi^2, \quad (2.13)$$

where $1/(4\pi \epsilon_0)$ is the Coulomb force constant.

2.2.3 Kerr Solution

A rotating uncharged black hole in 4-dimensional general relativity is described by the *Kerr solution*. In Boyer–Lindquist coordinates, the line element is

$$ds^2 = - \left(1 - \frac{2Mr}{\Sigma} \right) dt^2 - \frac{4aMr \sin^2 \theta}{\Sigma} dt d\phi + \frac{\Sigma}{\Delta} dr^2 + \Sigma d\theta^2 + \left(r^2 + a^2 + \frac{2a^2 Mr \sin^2 \theta}{\Sigma} \right) \sin^2 \theta d\phi^2, \quad (2.16)$$

where $\Sigma = r^2 + a^2 \cos^2 \theta$, $\Delta = r^2 - 2Mr + a^2$, $a = J/M$, and J is the spin angular momentum of the black hole. It is often convenient to introduce the dimensionless spin parameter $a_* = a/M = J/M^2$.

As in the Reissner–Nordström metric, there are two solutions for the equation $g^{rr} = 0$; that is

$$r_{\pm} = M \pm \sqrt{M^2 - a^2}. \quad (2.17)$$

r_+ is the radius of the event horizon, which requires $|a| \leq M$. For $|a| > M$ there is no horizon and the spacetime has a naked singularity at $r = 0$. It is worth noting that the topology of the spacetime singularity in the Kerr solution is different from that in the Schwarzschild and Reissner–Nordström spacetimes. It is still a curvature singularity and a singularity in the sense of geodesics incompleteness, but this is true only in the equatorial plane. In particular, geodesics outside the equatorial plane can reach the singularity and extend to another universe. The Kretschmann scalar \mathcal{K} is

$$\mathcal{K} = \frac{48M^2}{\Sigma^6} (r^6 - 15a^2 r^4 \cos^2 \theta + 15a^4 r^2 \cos^4 \theta - a^6 \cos^6 \theta), \quad (2.18)$$

and we can see that \mathcal{K} diverges at $r = 0$ only for $\theta = \pi/2$.

Let us consider the Kerr–Schild coordinates (t', x, y, z) , which are related to the Boyer–Lindquist ones by

$$\begin{aligned} x + iy &= (r + ia) \sin \theta \exp \left[i \int d\phi + i \int \frac{a}{\Delta} dr \right], \\ z &= r \cos \theta, \\ t' &= \int dt - \int \frac{r^2 + a^2}{\Delta} dr - r, \end{aligned} \quad (2.19)$$

where i is the imaginary unit, namely $i^2 = -1$. r is implicitly given by

$$r^4 - (x^2 + y^2 + z^2 - a^2) r^2 - a^2 z^2 = 0. \quad (2.20)$$

The singularity at $r = 0$ and $\theta = \pi/2$ corresponds to $z = 0$ and $x^2 + y^2 = a^2$, namely it is a ring. It is possible to extend the spacetime to negative r , and the ring connects two universes. However, the region $r < 0$ possesses closed time-like curves, which means it is possible to go backward in time. More details can be found, for instance, in [9].

As in the Reissner–Nordström case, the inner horizon r_- is likely unstable, but in the Kerr metric there is not a definitive proof. This would make the Kerr solution for $r < r_-$ physically not relevant.

2.2.4 No-Hair Theorem

The most general case of a rotating and electrically charged black hole is described by the *Kerr–Newman solution*. In analogy with the Reissner–Nordström metric, it can be obtained from the line element (2.16) with the substitution $M \rightarrow M - Q^2/(2r)$. The horizon is located at

$$r_+ = M + \sqrt{M^2 - Q^2 - a^2}, \quad (2.21)$$

and exists for $\sqrt{Q^2 + a^2} \leq M$.

The *no-hair theorem* asserts that black holes have only three asymptotic charges (the mass M , the spin angular momentum J , and the electric charge Q of the compact object) and no more. There are a number of assumptions behind this assertion. The spacetime must be stationary, asymptotically flat, and have 4 dimensions; the exterior region must be regular (no naked singularities and/or closed time-like curves); matter is described by the energy-momentum tensor of the electromagnetic field (but the theorem still holds in the presence of many other fields). For more details, see, e.g., [11]. The no-hair theorem was pioneered in the late 1960s and early 1970s by Israel [28], Carter [8], and Robinson [53], and its final form is still a work in progress. The name no-hair is to indicate that black holes have no features (hairs), although, to be precise, black holes can have three hairs (M , J , and Q). The fact that there is only the Kerr–Newman solution is the result of the *uniqueness theorem*. In the context of tests of the Kerr metric and of general relativity, both theorems are relevant. For instance, as a matter of principle, one may have different classes of black holes (each with characteristic M , J , and Q hairs), thus violating the uniqueness theorem, without any violation of the no-hair theorem.

2.3 Beyond the No-Hair Theorem

The no-hair theorem holds under specific assumptions. For instance, if the spacetime has more than 4 dimensions, there are also other kinds of black holes, e.g. the Myers–Perry black holes [44], as well as other “black objects” [16, 17]; see, for instance,

the review article [18]. In an n -dimensional spacetime, a Myers-Perry black hole is characterized by the mass M and other $(n - 1)/2$ parameters if n is odd, $n/2$ parameters if n is even, associated to the independent components of the angular momentum. So the number of hairs increases with n . “Hairy” black holes naturally arise also in the presence of non-Abelian gauge fields [58, 59].

In some alternative theories of gravity, the theorem may still holds, and an example is a simple scalar-tensor theory, in which the black hole solutions are the same as in general relativity [54]. Roughly speaking, this is because the Kerr metric is solution of the field equations

$$R_{\mu\nu} = 0, \quad (2.22)$$

and even the field equations of other theories of gravity may reduce to this simple form in the vacuum [52].

In other frameworks, the black hole solutions of general relativity may still be solutions of the new field equations, but their uniqueness is not guaranteed. A relevant example of violation of the no-hair theorem is presented in [25], where the authors discovered a family of hairy black holes in 4-dimensional Einstein’s gravity minimally coupled to a complex, massive scalar field. Here hairy black holes are possible by introducing a specific harmonic time-dependence in the scalar field, while the spacetime metric and the energy-momentum tensor of the scalar field are still stationary. There are also cases, like dynamical Chern–Simons gravity, in which non-rotating black holes are described by the Schwarzschild solution, but rotating black holes are not those of Kerr [65].

In general, we can distinguish two kinds of hairs, called, respectively, primary and secondary hairs. *Primary hairs* are real hairs of the black hole: if such hairs were to exist, then M , J , and Q would not completely characterize the compact object, and one or more additional parameters would be necessary. An example is a 5-dimensional Myers-Perry black hole: it is the 5-dimensional generalization of Kerr black holes and it has two angular momenta, so one more hair: J' [44].

Secondary hairs are instead related to some new charge that is common to all black holes. For instance, in Einstein-dilaton-Gauss-Bonnet gravity, a black hole has a scalar charge proportional to the volume integral of the Gauss–Bonnet invariant [33, 40]; that is, the scalar charge is determined by the black hole mass and it is not an additional degree of freedom.

In alternative theories of gravity, there may be further complications and the phenomenology can be much richer. For instance, some theories may not have black hole solutions. An example is the model of massive gravity discussed in [1]. The static and spherically symmetric vacuum solution of the corresponding field equations does not describe a black hole but a naked singularity.

In some theories even the definition of black hole may be problematic. For instance, in models with violation of the Lorentz symmetry, null geodesics may depend on the energy of the massless particle. In this case, there are different “event horizons” for photons with different energies, and it is possible that some high energy photons can always escape to infinity, so that there is no real black hole.

It is also possible that some frameworks have black hole solutions, but there is no mechanism to create black holes. In general relativity, black holes emerge as exact solutions of the Einstein equations. However, this is not enough to say that such solutions are physically relevant. In general relativity, we know that black holes can form from gravitational collapse and we have also some simple analytical models that show how this is possible (see Sect. 2.4). In some alternative theories, the gravitational collapse may simply be unable to create a black hole. For instance, black holes may be unstable solutions or would require a set-up impossible to realize. A possible example is represented by the model discussed in [67].

In general, black hole solutions in alternative theories of gravity are known in the non-rotating limit, either in analytic or numerical form, because static and spherically symmetric solutions are relatively easy to find. In some cases, analytic slow-rotating solutions have been found, see e.g. [38, 48, 64, 65]. Exact rotating black hole solutions, especially in analytic form, are more difficult to obtain [34]. This is actually true even in general relativity, and it is proved by the fact that the Kerr metric was discovered more than 45 years after the Schwarzschild solution.

2.4 Gravitational Collapse

When a star exhausts all its nuclear fuel, the gas pressure cannot balance the star own weight, and the body shrinks to find a new equilibrium configuration. For most stars, the pressure of degenerate electrons stops the collapse and the star becomes a white dwarf. However, if the collapsing part of the star is too heavy, the mechanism does not work, matter reaches higher densities, and protons and electrons transform into neutrons. If the pressure of degenerate neutrons stops the collapse, the star becomes a neutron star. If the collapsing core is still too massive and even the neutron pressure cannot stop the process, there is no known mechanism capable of finding a new equilibrium configuration, and the body should undergo a complete collapse. In this case, the final product is a black hole.

The aim of this section is to present the simplest and the next-to-simplest gravitational collapse models. These solutions are analytic and nicely show how the gravitational collapse of a spherically symmetric cloud of dust creates a spacetime singularity and an event horizon. For a review, see e.g. [32]. Numerical simulations can treat more realistic models, where the final product is still a black hole [2, 3].

We want to consider a spherically symmetric collapse, so the spacetime must be spherically symmetric. This means the metric is invariant under the group of spatial rotations $SO(3)$ and we can define the 2-dimensional metric induced on the unit 2-sphere as

$$d\Omega^2 = d\theta^2 + \sin^2\theta d\phi^2. \quad (2.23)$$

We introduce the function R such that $4\pi R^2$ represents the area of each 2-sphere in the spacetime. The 4-dimensional line element reads

$$ds^2 = g_{ab}dx^a dx^b + R^2 d\Omega^2, \quad (2.24)$$

where $a, b = 0, 1$ and R is a function of x^0 and x^1 . Choosing $x^0 = t$ and $x^1 = r$ and diagonalizing g_{ab} , we find that the most general line element of a spherically symmetric spacetime can be written as

$$ds^2 = -e^{2\lambda} dt^2 + e^{2\psi} dr^2 + R^2 d\Omega^2, \quad (2.25)$$

where λ , ψ , and R are functions of t and r only.

Let us assume that the collapsing body can be described by a perfect fluid. The coordinate system of the line element in Eq. (2.25) is called comoving because the coordinates t and r are “attached” to every collapsing particle. This is the rest-frame of the collapsing fluid and therefore the fluid 4-velocity is $u^\mu = (e^{-\lambda}, 0, 0, 0)$. The energy momentum tensor is

$$T^\mu_\nu = \text{diag}(\rho, P, P, P), \quad (2.26)$$

where ρ and P are, respectively, the energy density and the pressure of the fluid.

With the line element in Eq. (2.25), the Einstein tensor reads

$$G^t_t = -\frac{F'}{R^2 R'} + \frac{2\dot{R}e^{-2\lambda}}{R R'} (\dot{R}' - \dot{R}\lambda' - \dot{\psi}R'), \quad (2.27)$$

$$G^r_r = -\frac{\dot{F}}{R^2 \dot{R}} - \frac{2R'e^{-2\psi}}{R \dot{R}} (\dot{R}' - \dot{R}\lambda' - \dot{\psi}R'), \quad (2.28)$$

$$G^t_r = -e^{2\psi-2\lambda} G^r_t = \frac{2e^{-2\lambda}}{R} (\dot{R}' - \dot{R}\lambda' - \dot{\psi}R'), \quad (2.29)$$

$$G^\theta_\theta = G^\phi_\phi = \frac{e^{-2\psi}}{R} [(\lambda'' + \lambda'^2 - \lambda'\psi')R + R'' + R'\lambda' - R'\psi'] + \quad (2.30)$$

$$-\frac{e^{-2\lambda}}{R} [(\psi\ddot{R} + \dot{\psi}^2 - \dot{\lambda}\dot{\psi})R + \ddot{R} + \dot{R}\dot{\psi} - \dot{R}\dot{\lambda}]. \quad (2.31)$$

From the Einstein equations, we can get the following equations

$$G^t_t = 8\pi T^t_t \Rightarrow \frac{F'}{R^2 R'} = 8\pi\rho, \quad (2.32)$$

$$G^r_r = 8\pi T^r_r \Rightarrow \frac{\dot{F}}{R^2 \dot{R}} = -8\pi P, \quad (2.33)$$

$$G^t_r = 0 \Rightarrow \dot{R}' - \dot{R}\lambda' - \dot{\psi}R' = 0, \quad (2.34)$$

where the prime $'$ and the dot $\dot{}$ denote, respectively, the derivative with respect to r and t . F is the Misner-Sharp mass [41]

$$F = R(1 - e^{-2\psi} R'^2 + e^{-2\lambda} \dot{R}^2), \quad (2.35)$$

which is defined by the relation

$$1 - \frac{F}{R} = g_{\mu\nu} (\partial^\mu R) (\partial^\nu R) . \quad (2.36)$$

From Eq. (2.32), we can see that the Misner-Sharp mass is proportional to the gravitational mass within the radius r at the time t

$$F(r) = \int_0^r F' d\tilde{r} = 8\pi \int_0^r \rho R^2 R' d\tilde{r} = 2M(r) . \quad (2.37)$$

It is worth noting that $n^\mu = \partial^\mu R$ is the normal to the surface $R = \text{const.}$ Therefore, as seen in Sect. 2.1, when $1 - F/R = 0$, the surface $R = \text{const.}$ is a null surface (and defines the location of the apparent horizon in the dust collapse models in the next subsections).

A fourth relation can be obtained from the covariant conservation of the matter energy-momentum tensor

$$\nabla_\mu T^\mu_\nu = 0 \Rightarrow \lambda' = -\frac{P'}{\rho + P} . \quad (2.38)$$

2.4.1 Dust Collapse

For dust, $P = 0$, and Eqs. (2.32)–(2.34), and (2.38) become

$$\frac{F'}{R^2 R'} = 8\pi\rho , \quad (2.39)$$

$$\frac{\dot{F}}{R^2 \dot{R}} = 0 , \quad (2.40)$$

$$\dot{R}' - \dot{R}\lambda' - \dot{\psi} R' = 0 , \quad (2.41)$$

$$\lambda' = 0 . \quad (2.42)$$

Equation (2.40) shows that, in the case of dust, F is independent of t , namely there is no inflow or outflow through any spherically symmetric shell with radial coordinate r . This means that the exterior spacetime is described by the Schwarzschild solution. In the general case with $P \neq 0$, this may not be true, and the interior region must be matched with a non-vacuum Vaidya spacetime. If r_b is the comoving radial coordinate of the boundary of the cloud of dust, $F(r_b) = 2M$, where M is the Schwarzschild mass of the vacuum exterior.

Equation (2.42) implies that $\lambda = \lambda(t)$ and permits one to choose the time gauge in such a way that $\lambda = 0$. It is indeed always possible to define a new time coordinate \tilde{t} such that $d\tilde{t} = e^\lambda dt$ and therefore $g_{\tilde{t}\tilde{t}} = -1$.

Equation (2.41) becomes $\dot{R}' - \dot{\psi} R' = 0$ and we can write

$$R' = e^{g(r)+\psi} . \quad (2.43)$$

We introduce the function $f(r) = e^{2g(r)} - 1$ and Eq. (2.35) becomes

$$\dot{R}^2 = \frac{F}{R} + f . \quad (2.44)$$

The line element can now be written as

$$ds^2 = -dt^2 + \frac{R'^2}{1+f} dr^2 + R^2 d\Omega^2 . \quad (2.45)$$

This is the Lemaitre–Tolman–Bondi, or LTB, metric [6, 36, 56].

The Kretschmann scalar of the line element in (2.45) is

$$\mathcal{K} = 12 \frac{F'^2}{R^4 R'^2} - 32 \frac{F F'}{R^5 R'} + 48 \frac{F^2}{R^6} , \quad (2.46)$$

and diverges if $R = 0$. The system has a gauge degree of freedom that can be fixed by setting the scale at a certain time. It is common to set the area radius $R(t, r)$ to the comoving radius r at the initial time $t_i = 0$, namely $R(0, r) = r$, and introduce the scale factor a

$$R(t, r) = ra(t, r) . \quad (2.47)$$

We have thus $a = 1$ at $t = t_i$ and $a = 0$ at the time of the formation of the singularity. The condition for collapse is $\dot{a} < 0$. From Eq. (2.39), the regularity of the energy density at the initial time t_i requires to write the Misner–Sharp mass as $F(r) = r^3 m(r)$, where $m(r)$ is a sufficiently regular function of r in the interval $[0, r_b]$. Equation (2.39) becomes

$$\rho = \frac{3m + rm'}{a^2 (a + ra')} . \quad (2.48)$$

The function $m(r)$ is usually written as a polynomial expansion around $r = 0$

$$m(r) = \sum_{k=0}^{\infty} m_k r^k , \quad (2.49)$$

where $\{m_k\}$ are constants. Requiring that the energy density ρ has no cusps at $r = 0$, $m_1 = 0$.

From Eq. (2.46), we see that the Kretschmann scalar diverges even when $R' = 0$ if $m' \neq 0$. However, the nature of these singularities is different: they arise from the overlapping of radial shells and are called shell crossing singularities [24]. Here the radial geodesic distance between shells with radial coordinates r and $r + dr$

vanishes, but the spacetime may be extended through the singularity by a suitable redefinition of the coordinates. To avoid any problem, it is common to impose that the collapse model has no shell crossing singularities, for instance requiring that $R' \neq 0$ or that m'/R' does not diverge.

At the initial time t_i , Eq. (2.44) becomes

$$\dot{a}(t_i, r) = -\sqrt{m + \frac{f}{r^2}}, \quad (2.50)$$

and we can see that the choice of f corresponds to the choice of the initial velocity profile of the particles in the cloud. In order to have a finite velocity at all radii, it is necessary to impose some conditions on f . It is common to write $f(r) = r^2 b(r)$ and $b(r)$ as a polynomial expansion around $r = 0$:

$$b(r) = \sum_{k=0}^{\infty} b_k r^k. \quad (2.51)$$

2.4.2 Homogeneous Dust Collapse

The simplest model of gravitational collapse is the Oppenheimer-Snyder model [46]. It describes the collapse of a homogeneous and spherically symmetric cloud of dust. In this case, $\rho = \rho(t)$ is independent of r , so $m = m_0$ and $b = b_0$. The interior metric is the time reversal of the Friedmann–Robertson–Walker solution

$$ds^2 = -dt^2 + a^2 \left(\frac{dr^2}{1 + b_0 r^2} + r^2 d\Omega^2 \right). \quad (2.52)$$

$b_0 = 0$ is the counterpart of a flat universe and corresponds to a marginally bound collapse, namely the scenario in which the falling particles have vanishing velocity at infinity. Equation (2.44) becomes

$$\dot{a} = -\sqrt{\frac{m_0}{a} + b_0}. \quad (2.53)$$

For $b_0 = 0$, the solution is

$$a(t) = \left(1 - \frac{3\sqrt{m_0}}{2} t \right)^{2/3}. \quad (2.54)$$

The formation of the singularity occurs at the time

$$t_s = \frac{2}{3\sqrt{m_0}}. \quad (2.55)$$

The curve $t_{\text{ah}}(r)$ describing the time at which the shell r crosses the apparent horizon can be obtained from

$$1 - \frac{F}{R} = 1 - \frac{r^2 m_0}{a} = 0. \quad (2.56)$$

For $b_0 = 0$, the solution is

$$t_{\text{ah}}(r) = t_{\text{s}} - \frac{2}{3}F = \frac{2}{3\sqrt{m_0}} - \frac{2}{3}r^3 m_0. \quad (2.57)$$

The Finkelstein diagram of the gravitational collapse of a homogeneous and spherically symmetric cloud of dust is sketched in Fig. 2.2. At the time $t = t_0$, the radius of the surface of the cloud crosses the Schwarzschild radius. We have the formation of both the event horizon in the exterior region and the apparent horizon at the boundary $r = r_b$, i.e. $t_0 = t_{\text{ah}}(r_b)$. As shown in Fig. 2.2, the exterior region is now settled down to the static Schwarzschild spacetime, while the radius of the apparent horizon propagates to smaller radii and reaches $r = 0$ at the time of the formation of the singularity t_s .

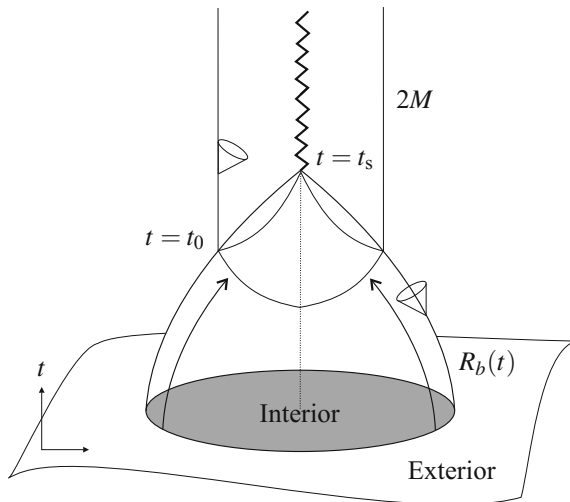


Fig. 2.2 Finkelstein diagram for the gravitational collapse of a homogeneous and spherically symmetric cloud of dust. $R_b(t)$ is the radius of the cloud (in the Schwarzschild coordinates of the exterior region) and separates the interior from the vacuum exterior. The cloud collapses as t increases and at the time $t = t_0$ the horizon forms at the boundary when $R_b(t_0) = 2M$. In the interior, the apparent horizon propagates inwards and reaches the center of symmetry at the time of the formation of the singularity $t = t_s$. For $t > t_s$, the spacetime has settled down to the usual Schwarzschild solution. Figure courtesy of Daniele Malafarina

2.4.3 Inhomogeneous Dust Collapse

In the inhomogeneous dust collapse scenario, ρ depends on both t and r , so we have $m = m(r)$, $b = b(r)$, and $a = a(t, r)$. While the Hawking-Penrose singularity theorems assure that, under certain conditions, the formation of a singularity is inevitable after the formation of an apparent horizon [23], the picture of the collapse may be different from the simple Oppenheimer-Snyder model. In particular, it is possible that the singularity is naked for an infinitesimal time, namely there may be null geodesics that start from the singularity and go to null infinity, see e.g. [10, 31, 45, 63].

If we want to impose that the energy density has no cusps at the center, $m_1 = 0$ and the simplest form of the function m is

$$m(r) = m_0 + m_2 r^2. \quad (2.58)$$

Now the density profile is described by two parameters, m_0 and m_2 . Imposing the condition that ρ must be a decreasing function of r (the density of the cloud is higher at the center and lower at larger radii), $m_2 < 0$.

Equation (2.44) is now

$$\dot{a} = -\sqrt{\frac{m}{a}} + b. \quad (2.59)$$

In the marginally bound case $b = 0$, the solution is

$$a(t, r) = \left(1 - \frac{3\sqrt{m(r)}}{2}t\right)^{2/3}, \quad (2.60)$$

and we see that each shell collapses with a different scale factor and a different velocity. The singularity and the apparent horizon are now described by the curves

$$t_s(r) = \frac{2}{3\sqrt{m}} \quad (2.61)$$

$$t_{\text{ah}}(r) = \frac{2}{3\sqrt{m}} - \frac{2}{3}r^3 m. \quad (2.62)$$

If $m = m_0 + m_2 r^2$, we find

$$t_s(r) = \frac{2}{3\sqrt{m_0 + m_2 r^2}} \quad (2.63)$$

$$t_{\text{ah}}(r) = \frac{2}{3\sqrt{m_0 + m_2 r^2}} - \frac{2}{3}r^3 (m_0 + m_2 r^2). \quad (2.64)$$

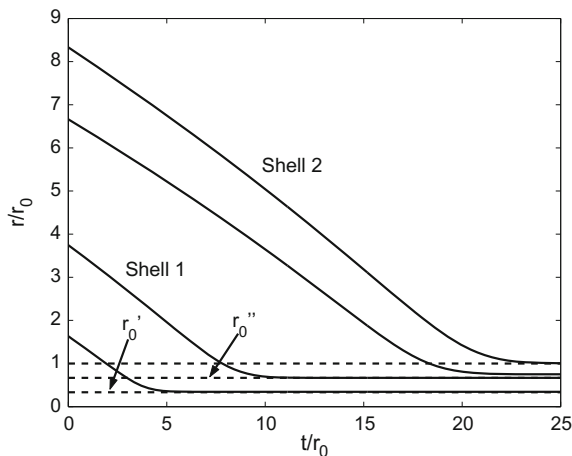


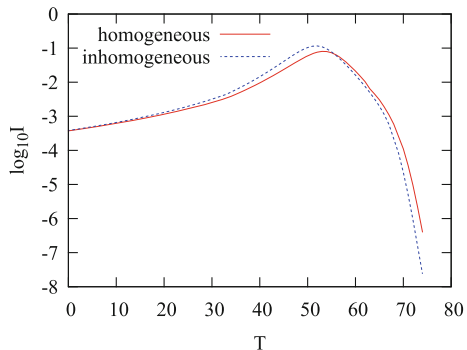
Fig. 2.4 Evolution of the radial coordinates of the inner and of the outer boundaries of shell 1 and shell 2 (solid lines) with respect to the time t of a distant observer. The three horizontal dashed lines indicate the coordinate of the horizon before the collapse of shell 1 ($r'_0 = 2M$, lower line), after the collapse of shell 1 and before the collapse of shell 2 ($r''_0 = 2M + 2M_1$, central line), and after the collapse of shell 2 ($r_0 = 2M + 2M_1 + 2M_2$, upper line). M , M_1 , and M_2 are, respectively, the mass of the pre-existing black hole, of shell 1, and of shell 2. See the text for more details. From [37] under the terms of the Creative Commons Attribution License

The picture of gravitational collapse as seen by a distant observer can be understood within the toy-models discussed in [37, 66]. Let us consider a pre-existing black hole of mass M and two spherically symmetric shells of matter collapsing onto the black hole and with the mass, respectively, M_1 and M_2 . The two shells have a finite thickness, so each shell has inner and outer boundaries. The evolution of such a system is shown in Fig. 2.4.

At the beginning, we have the pre-existing black hole and the two shells at large radii. The event horizon of the black hole is at $r'_0 = 2M$. After the collapse of shell 1, the horizon of the new black hole is at $r''_0 = 2M + 2M_1$. However, the distant observer does not see (for the moment) the outer boundary of shell 1 crossing the horizon r''_0 . The radius of the outer boundary of shell 1 seems to asymptotically approach r''_0 , due to the infinite gravitational redshift. Then we have the collapse of shell 2. Now the horizon of the black hole is at $r_0 = 2M + 2M_1 + 2M_2$ and the distant observer does not see the outer boundary of shell 2 crossing the surface at the radial coordinate r_0 .

Let us notice that the radiation emitted by the most outer boundary of any collapsing configuration is more and more redshifted, so that any distant observer eventually sees a black hole for any practical purpose (even if the analytical formula predicts a non-zero emission of radiation at any time). The calculations of the radiation emitted by a collapsing body within some simple toy-models are presented in [35]. The light curves for a homogeneous and inhomogeneous, spherically symmetric, collapsing balls of dust are shown in Fig. 2.5. At late times, the emission of radiation is exponentially suppressed.

Fig. 2.5 Light curves of a homogeneous (red solid curve) and inhomogeneous (blue dashed curve), spherically symmetric, collapsing balls of dust assuming a simple model of emission. Time T in units $2M = 1$; luminosity in arbitrary units. From [35] under the terms of the Creative Commons Attribution License



2.5 Beyond the Standard Picture

It is natural to expect that the singularity at the center of black holes is due to the breakdown of the classical theory and that it should be removed when unknown quantum gravity effects are taken into account. If we believe that the energy scale of quantum gravity is the Planck mass M_{Pl} , we may expect that the Kretschmann scalar is bounded by

$$\mathcal{K} \lesssim \frac{1}{M_{\text{Pl}}^4}. \quad (2.65)$$

From Eq. (2.7), we see that new physics should show up at the radius

$$r \approx (M M_{\text{Pl}}^2)^{1/3}. \quad (2.66)$$

However, as already mentioned in Sect. 2.2, charged or rotating black holes have the inner horizon at $r = r_-$, which is unstable. This means that deviations from these metrics should be at least at r_- . In the case of extremal or almost extremal objects, r_- approaches r_+ , and therefore new physics may be not far from the event horizon.

There are also arguments suggesting that black holes may be macroscopic quantum objects. Roughly speaking, the identification of the Planck scale as the fundamental energy scale of quantum gravity arises when we quantize general relativity and find the problems of unitarity and renormalizability. The theory looks like a good effective theory at low energies, namely for energies $E \ll M_{\text{Pl}}$, but it breaks down when E approaches M_{Pl} . However, this conclusion is obtained by considering the scattering of two particles. In a system made of many components, it is possible that the actual scale of quantum gravity is given by the gravitational radius $\sim M$, where M is the mass/energy of the system, see e.g. [14, 15, 21, 39]. In these scenarios, the metric description typically breaks down inside the black hole.

If the metric description holds at the center of black holes, we can imagine two ways to solve the central singularity, in the sense that geodesics do not stop at $r = 0$

and predictability is not lost. One of these possibilities is a wormhole-like solution. In this scenario, the singularity is replaced by a “throat” connecting two universes. For a static/stationary black hole solution, we can have a wormhole, namely a topologically non-trivial structure connecting two asymptotically flat universes. In the case of a black hole formed from gravitational collapse, the throat can connect the original universe to a baby universe generated by the gravitational collapse inside the black hole. The alternative possibility to solve the singularity is to have a spacetime in which the center $r = 0$ can never be reached in a finite time (with a finite value of the affine parameter in the case of null geodesics). These are the two natural scenarios to solve the central singularity, and there are not more, because one has to preserve the property that, roughly speaking, inside a black hole everything must fall to its center. The problem of a geodesically incomplete spacetime can thus be fixed either postulating the extension of the spacetime beyond $r = 0$ or the impossibility of reaching $r = 0$ in a finite time. Other solutions seem at least to require more exotic physics.

The quantum gravity inspired models studied in [4, 5, 20, 67] are characterized by the fact that gravity becomes repulsive at very high densities. The result is that the singularity is replaced by a bounce, after which the collapsing matter starts expanding. In principle, we may have two scenarios: (i) there is a bounce and the creation of a baby universe inside the black hole, or (ii) there is no black hole, in the sense that the collapse only creates an apparent horizon, which can be interpreted as a black hole for a while by the exterior observer if the observational time is shorter than the time scale of the evolution of the process.

In general, both scenarios may be possible, and it depends on the specific model. The scenario (i) is not easy to realize. A similar spacetime can be obtained with a cut-and-paste procedure, in which a singular manifold is extended beyond the singularity by removing the singularity and sewing the spacetime to a new non-singular manifold describing an expanding baby universe. However, this is possible only in very simple examples. Matching of the two manifolds involves the continuity of the first and second fundamental forms across some hypersurface, which is not possible in general due to the lack of a sufficient number of free parameters.

In the case of the scenario (ii) and under certain conditions, the lifetime of the apparent horizon might exactly scale as the Hawking evaporation time. It is thus possible to argue a link between instability of this kind of objects and Hawking radiation [5].

2.6 Penrose Diagrams

Penrose diagrams are 2-dimensional spacetime diagrams used to figure out the global properties and the causal structure of asymptotically flat spacetimes. Since they are 2-dimensional diagrams, every point represents a 2-dimensional sphere of the original 4-dimensional spacetime. Penrose diagrams are obtained by a conformal transformation of the original coordinates such that the entire spacetime is transformed into

a compact region. Since the transformation is conformal, angles are preserved, and null geodesics remain lines at 45° . Time-like geodesics are inside the light-cone, space-like geodesics are outside. A more detailed discussion on the topic can be found, for instance, in [57, 62].

It is probably easier to start from the simplest example, namely the Penrose diagram for the Minkowski spacetime. In spherical coordinates (t, r, θ, ϕ) , the line elements is

$$ds^2 = -dt^2 + dr^2 + r^2 d\theta^2 + r^2 \sin^2 \theta d\phi^2. \quad (2.67)$$

We perform the following conformal transformation

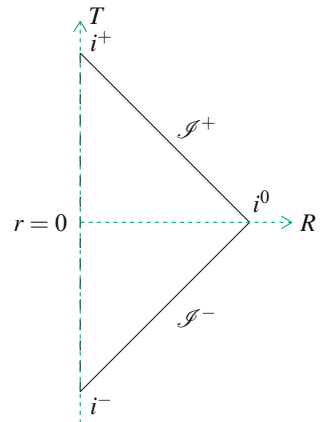
$$\begin{aligned} t &= \frac{1}{2} \tan \frac{T+R}{2} + \frac{1}{2} \tan \frac{T-R}{2}, \\ r &= \frac{1}{2} \tan \frac{T+R}{2} - \frac{1}{2} \tan \frac{T-R}{2}, \end{aligned} \quad (2.68)$$

where the use of the tangent function \tan is to bring points at infinity to points at a finite value in the new coordinates. The line element now reads

$$\begin{aligned} ds^2 &= \left(4 \cos^2 \frac{T+R}{2} \cos^2 \frac{T-R}{2} \right)^{-1} (-dT^2 + dR^2) \\ &\quad + r^2 d\theta^2 + r^2 \sin^2 \theta d\phi^2. \end{aligned} \quad (2.69)$$

The Penrose diagram for the Minkowski spacetime is shown in Fig. 2.6. The semi-infinite (t, r) plane is now a triangle. The dashed vertical line is the origin $r = 0$. Every point corresponds to the 2-sphere (θ, ϕ) . There are five different asymptotic regions. Without a rigorous treatment, they can be defined as follows:

Fig. 2.6 Penrose diagram for the Minkowski spacetime. See the text for the details



Future time-like infinity i^+ : the region toward which time-like geodesics extend. It corresponds to the points at $t \rightarrow \infty$ with finite r .

Past time-like infinity i^- : the region from which time-like geodesics come. It corresponds to the points at $t \rightarrow -\infty$ with finite r .

Spatial infinity i^0 : the region toward which space-like slices extend. It corresponds to the points at $r \rightarrow \infty$ with finite t .

Future null infinity \mathcal{I}^+ : the region toward which outgoing null geodesics extend. It corresponds to the points at $t + r \rightarrow \infty$ with finite $t - r$.

Past null infinity \mathcal{I}^- : the region from which ingoing null geodesics come. It corresponds to the points at $t - r \rightarrow -\infty$ with finite $t + r$.

Such asymptotic regions are points or segments in the Penrose diagram and their T and R coordinates are:

$$\begin{aligned} i^+ \quad T &= \pi, \quad R = 0. \\ i^- \quad T &= -\pi, \quad R = 0. \\ i^0 \quad T &= 0, \quad R = \pi, \end{aligned} \tag{2.70}$$

and

$$\begin{aligned} \mathcal{I}^+ \quad T + R &= \pi, \quad T - R \in (-\pi; \pi). \\ \mathcal{I}^- \quad T - R &= -\pi, \quad T + R \in (-\pi; \pi). \end{aligned} \tag{2.71}$$

Penrose diagrams become a powerful tool to explore the global properties and the causal structure of more complicated spacetimes. The simplest non-trivial example is the Schwarzschild spacetime. If we consider its maximal extension in Kruskal–Szekeres coordinates and we perform the following coordinate transformation

$$\begin{aligned} V &= \frac{1}{2} \tan \frac{T+R}{2} + \frac{1}{2} \tan \frac{T-R}{2}, \\ U &= \frac{1}{2} \tan \frac{T+R}{2} - \frac{1}{2} \tan \frac{T-R}{2}, \end{aligned} \tag{2.72}$$

the line element becomes

$$\begin{aligned} ds^2 &= \frac{32M^3}{r} e^{-r/(2M)} \left(4 \cos^2 \frac{T+R}{2} \cos^2 \frac{T-R}{2} \right)^{-1} (-dT^2 + dR^2) \\ &\quad + r^2 d\theta^2 + r^2 \sin^2 \theta d\phi^2. \end{aligned} \tag{2.73}$$

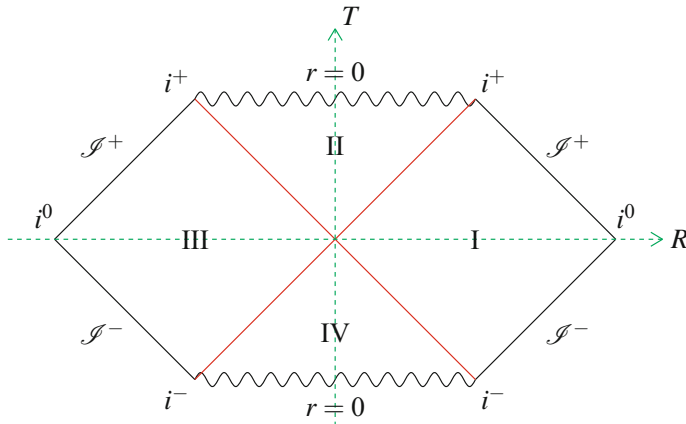


Fig. 2.7 Penrose diagram for the maximal extension of the Schwarzschild spacetime. See the text for the details

The Penrose diagram of the maximal extension of the Schwarzschild spacetime is shown in Fig. 2.7. The asymptotic regions i^+ , i^- , i^0 , \mathcal{I}^+ , and \mathcal{I}^- are those already found in the Minkowski case. We can distinguish four regions, indicated, respectively, by I, II, II, and IV in the figure.

The region I corresponds to our universe, namely the exterior region of the Schwarzschild spacetime in Schwarzschild coordinates. The region II is the black hole, so the Schwarzschild spacetime in Schwarzschild coordinates has only the regions I and II. The central singularity of the black hole at $r = 0$ is represented by the line with wiggles above the region II and the diagram clearly shows it is a space-like singularity.⁴ The event horizon of the black hole at $r = 2M$ is the red line at 45° (it is indeed a null surface) separating the regions I and II. Any ingoing light ray in the region I is captured by the black hole, while any outgoing light ray in the region I reaches future null infinity \mathcal{I}^+ . Null and time-like geodesics in the region II cannot exit the black hole and they necessarily fall to the singularity at $r = 0$.

The regions III and IV emerge from the extension of the Schwarzschild spacetime. The region III corresponds to another universe. The red line at 45° separating the regions II and III is the event horizon of the black hole at $r = 2M$. Like in the region I, any light ray in the region III can either cross the event horizon or escape to infinity. No future-oriented null or time-like geodesics can escape from the region II. Our universe in the region I and the other universe in the region III cannot communicate: no null or time-like geodesic can go from one region to another.

⁴Singularities, like trajectories, can be space-like, null, or time-like, depending on their causal properties. Space-like singularities are represented by lines with an inclination lower than 45° (like space-like trajectories). Time-like singularities are represented by lines with an inclination higher than 45° (like time-like trajectories). The singularity at $r = 0$ in the Penrose diagram of the Schwarzschild solution is represented by a horizontal line and is thus space-like. For more details, see e.g. [19] and references therein.

Fig. 2.8 Penrose diagram for the complete collapse of a homogeneous cloud of dust, corresponding to the situation in Fig. 2.2. The letter S indicates the interior region of the collapsing star and the black arc extending from i^- to $r = 0$ is its boundary. See the text for the details

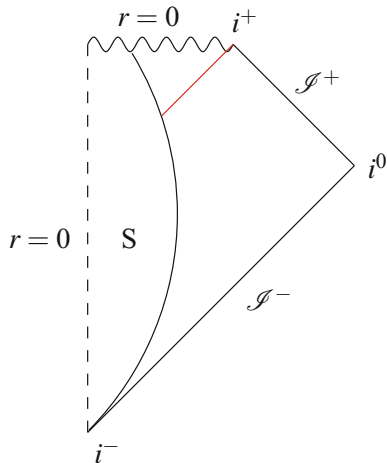
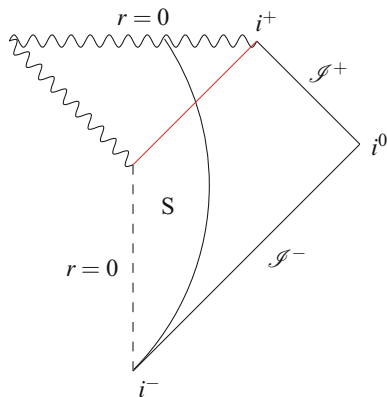


Fig. 2.9 Penrose diagram for the complete collapse of an inhomogeneous cloud of dust with a temporary naked singularity, namely the situation in Fig. 2.3. The letter S indicates the interior region of the collapsing star and the *black arc* extending from i^- to $r = 0$ is its boundary. See the text and [43, 47] for the details.



The region IV is a *white hole*. If a black hole is a region of the spacetime where null and time-like geodesics can only enter and never exit, a white hole is a region where null and time-like geodesics can only exit and never enter. The red lines at 45° separating the region IV from the regions I and III are the horizons at $r = 2M$ of the white hole.

Figure 2.7 is the Penrose diagram for the maximal extension of the Schwarzschild solution, which is static. However, black holes in the Universe should be created from gravitational collapse of massive bodies. The corresponding Penrose diagrams are shown in Figs. 2.8 and 2.9 and are substantially different from the diagram in Fig. 2.7. Figure 2.8 is for the case of the collapse of a homogeneous cloud of dust (the Penrose diagram corresponding to the Finkelstein diagram in Fig. 2.2): the singularity is created at the same time $t = t_s$ for all shells. Figure 2.9 shows the collapse of an inhomogeneous cloud of dust with the formation of a temporary naked singularity

(the counterpart of the Finkelstein diagram in Fig. 2.3) [43, 47]: here the singularity is created first at the center and, for an infinitesimal time, is naked.

The Penrose diagram for a static spacetime with a massive body would be equivalent to that for the Minkowski spacetime in Fig. 2.6. In the case of a collapsing body, the diagram changes when the radius of the body crosses the corresponding Schwarzschild radius at $r = 2M$. At this point, we have the formation of the event horizon, represented by the red line at 45° in Figs. 2.8 and 2.9. Now the exterior region looks like the region I in the Penrose diagram of the Schwarzschild spacetime with the future null infinity \mathcal{I}^+ . In the interior region, the radius of the body goes to the space-like singularity at $r = 0$. There is no white hole or parallel universe.

Figures 2.8 and 2.9 show the Penrose diagrams of two examples of complete collapse in classical general relativity. The picture changes when we consider “quantum” effects, broadly defined. The left diagram in Fig. 2.10 is the Penrose diagram for the formation of a black hole from the collapse of a star and its “complete evaporation” due to Hawking radiation. Even in this case, the event horizon is represented by a red line at 45° . While the evaporation process progressively reduces the radius of the horizon and the object emits radiation moving along null geodesics, as an artifact of the conformal transformation the horizon is still a line at 45° and it seems like all Hawking radiation is emitted together at once. In the case of complete evaporation, the upper part of the Penrose diagram is like that of the Minkowski spacetime.

The right diagram in Fig. 2.10 is one of the Penrose diagrams for the gravitational collapse with bounce studied in [4, 20]. The diagram is slightly different if the evaporation of the apparent horizon is associated to some Hawking-like process. In these scenarios, there is neither formation of black hole nor formation of spacetime

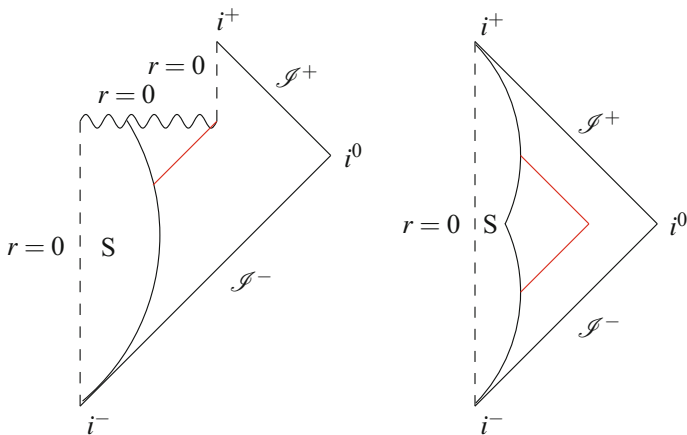


Fig. 2.10 Penrose diagrams for the formation and the Hawking evaporation of a *black hole* (left) and for the gravitational collapse with bounce and without formation of singularities (right). The letter *S* indicates the interior region of the collapsing star and the *black arc* extending from i^- is its boundary. See the text for the details

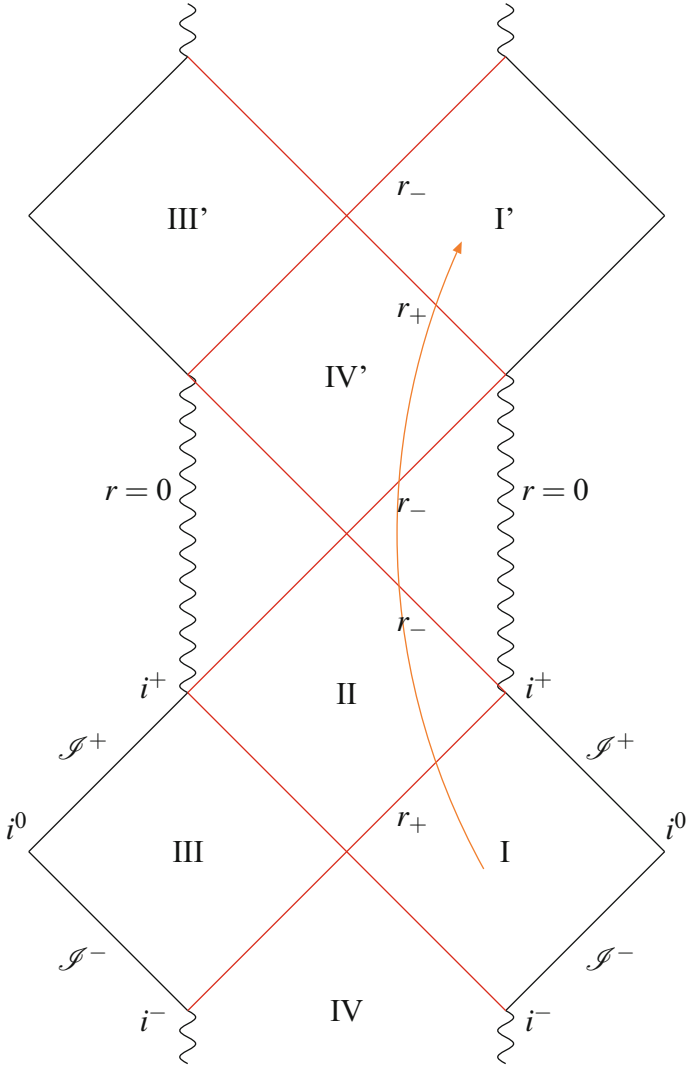


Fig. 2.12 Penrose diagram for the maximal extension of the Reissner–Nordström spacetime. See the text for the details

Figure 2.11 shows the Penrose diagram for the maximal extension of the Kerr spacetime. The region I is our universe outside the black hole and the red line at 45° separating the regions I and II and labeled by r_+ is the event horizon. As in the Schwarzschild spacetime, the region III is another universe and the region IV is a white hole. The region II is the black hole interior between the event horizon r_+ and the inner horizon r_- . The singularity at $r = 0$ is time-like (not space-like as in Schwarzschild) and therefore it is a vertical line and can be avoided by a test-particle.

A test-particle in the region I can cross the event horizon, cross the inner horizon, and then enter the ring singularity outside the equatorial plane (green trajectory). The latter is a “gate” to the region $\bar{\text{I}}$, which is an anti-universe at $r < 0$. Alternatively, the test-particle can cross the event horizon, cross the inner horizon, and then cross again the inner horizon to reach the region IV’, which is a white hole, to eventually enter the region I’ representing another universe (orange trajectory).

The Penrose diagram for the maximal extension of the Reissner–Nordström spacetime is shown in Fig. 2.12. It is very similar to the diagram in Fig. 2.11 for the Kerr solution, with the remarkable difference that the singularity at $r = 0$ is not a ring singularity and therefore the region $\bar{\text{I}}$ and $\bar{\text{III}}$ in Fig. 2.11 do not exist in the Reissner–Nordström spacetime.

References

1. S.V. Babak, L.P. Grishchuk, *Int. J. Mod. Phys. D* **12**, 1905 (2003), [arXiv:gr-qc/0209006](#)
2. L. Baiotti, I. Hawke, P.J. Montero, F. Löffler, L. Rezzolla, N. Stergioulas, J.A. Font, E. Seidel, *Phys. Rev. D* **71**, 024035 (2005), [arXiv:gr-qc/0403029](#)
3. L. Baiotti, L. Rezzolla, *Phys. Rev. Lett.* **97**, 141101 (2006), [arXiv:gr-qc/0608113](#)
4. C. Bambi, D. Malafarina, L. Modesto, *Eur. Phys. J. C* **74**, 2767 (2014), [arXiv:1306.1668 \[gr-qc\]](#)
5. C. Bambi, D. Malafarina, L. Modesto, *JHEP* **1604**, 147 (2016), [arXiv:1603.09592 \[gr-qc\]](#)
6. H. Bondi, *Mon. Not. Roy. Astron. Soc.* **107**, 410 (1947)
7. I. Booth, *Can. J. Phys.* **83**, 1073 (2005), [arXiv:gr-qc/0508107](#)
8. B. Carter, *Phys. Rev. Lett.* **26**, 331 (1971)
9. S. Chandrasekhar, *The Mathematical Theory of Black Holes* (Clarendon Press, Oxford, 1998)
10. D. Christodoulou, *Commun. Math. Phys.* **93**, 171 (1984)
11. P.T. Chrusciel, J.L. Costa, M. Heusler, *Living Rev. Rel.* **15**, 7 (2012), [arXiv:1205.6112 \[gr-qc\]](#)
12. P. Diener, *Class. Quant. Grav.* **20**, 4901 (2003), [arXiv:gr-qc/0305039](#)
13. S. Droz, *Phys. Rev. D* **55**, 3575 (1997)
14. G. Dvali, C. Gomez, *Fortsch. Phys.* **61**, 742 (2013), [arXiv:1112.3359 \[hep-th\]](#)
15. G. Dvali, C. Gomez, *Phys. Lett. B* **719**, 419 (2013), [arXiv:1203.6575 \[hep-th\]](#)
16. R. Emparan, *JHEP* **0403**, 064 (2004), [arXiv:hep-th/0402149](#)
17. R. Emparan, H.S. Reall, *Phys. Rev. Lett.* **88**, 101101 (2002), [arXiv:hep-th/0110260](#)
18. R. Emparan, H.S. Reall, *Living Rev. Rel.* **11**, 6 (2008), [arXiv:0801.3471 \[hep-th\]](#)
19. F. Fayos, R. Torres, *Class. Quant. Grav.* **28**, 215023 (2011), [arXiv:1204.4651 \[gr-qc\]](#)
20. V.P. Frolov, G.A. Vilkovisky, *Phys. Lett. B* **106**, 307 (1981)
21. S.B. Giddings, *Phys. Rev. D* **90**, 124033 (2014), [arXiv:1406.7001 \[hep-th\]](#)
22. S.W. Hawking, *Commun. Math. Phys.* **25**, 152 (1972)
23. S.W. Hawking, R. Penrose, *Proc. Roy. Soc. Lond. A* **314**, 529 (1970)
24. C. Hellaby, K. Lake, *Astrophys. J.* **290**, 381 (1985)
25. C.A.R. Herdeiro, E. Radu, *Phys. Rev. Lett.* **112**, 221101 (2014), [arXiv:1403.2757 \[gr-qc\]](#)
26. S. Hossenfelder, L. Smolin, *Phys. Rev. D* **81**, 064009 (2010), [arXiv:0901.3156 \[gr-qc\]](#)
27. S.A. Hughes, C.R. Keeton, P. Walker, K.T. Walsh, S.L. Shapiro, S.A. Teukolsky, *Phys. Rev. D* **49**, 4004 (1994)
28. W. Israel, *Phys. Rev.* **164**, 1776 (1967)
29. T. Jacobson, S. Venkataramani, *Class. Quant. Grav.* **12**, 1055 (1995), [arXiv:gr-qc/9410023](#)
30. T. Johannsen, *Phys. Rev. D* **87**, 124017 (2013), [arXiv:1304.7786 \[gr-qc\]](#)
31. P.S. Joshi, I.H. Dwivedi, *Phys. Rev. D* **47**, 5357 (1993), [arXiv:gr-qc/9303037](#)
32. P.S. Joshi, D. Malafarina, *Int. J. Mod. Phys. D* **20**, 2641 (2011), [arXiv:1201.3660 \[gr-qc\]](#)

33. P. Kanti, N.E. Mavromatos, J. Rizos, K. Tamvakis, E. Winstanley, Phys. Rev. D **54**, 5049 (1996), [arXiv:hep-th/9511071](#)
34. B. Kleihaus, J. Kunz, E. Radu, Phys. Rev. Lett. **106**, 151104 (2011), [arXiv:1101.2868](#) [gr-qc]
35. L. Kong, D. Malafarina, C. Bambi, Eur. Phys. J. C **74**, 2983 (2014), [arXiv:1310.8376](#) [gr-qc]
36. G. Lemaitre, Annales Soc. Sci. Brux. I A **53**, 51 (1933) [Gen. Rel. Grav. **29**, 641 (1997)]
37. Y. Liu, S.N. Zhang, Phys. Lett. B **679**, 88 (2009), [arXiv:0907.2574](#) [gr-qc]
38. A. Maselli, P. Pani, L. Gualtieri, V. Ferrari, Phys. Rev. D **92**, 083014 (2015), [arXiv:1507.00680](#) [gr-qc]
39. S.D. Mathur, Fortsch. Phys. **53**, 793 (2005), [arXiv:hep-th/0502050](#)
40. S. Mignemi, N.R. Stewart, Phys. Rev. D **47**, 5259 (1993), [arXiv:hep-th/9212146](#)
41. C.W. Misner, D.H. Sharp, Phys. Rev. **136**, B571 (1964)
42. C.W. Misner, K.S. Thorne, J.A. Wheeler, *Gravitation* (W. H. Freeman and Company, San Francisco, 1973)
43. U. Miyamoto, S. Jingan and T. Harada, PTEP **2013**, 053E01 (2013), [arXiv:1108.0248](#) [gr-qc]
44. R.C. Myers, M.J. Perry, Ann. Phys. **172**, 304 (1986)
45. R.P.A.C. Newman, Class. Quant. Grav. **3**, 527 (1986)
46. J.R. Oppenheimer, H. Snyder, Phys. Rev. **56**, 455 (1939)
47. N. Ortiz, O. Sarbach, Class. Quant. Grav. **28**, 235001 (2011), [arXiv:1106.2504](#) [gr-qc]
48. P. Pani, C.F.B. Macedo, L.C.B. Crispino, V. Cardoso, Phys. Rev. D **84**, 087501 (2011), [arXiv:1109.3996](#) [gr-qc]
49. R. Penrose, Proc. Roy. Soc. Lond. A **284**, 159 (1965)
50. E. Poisson, *A Relativists Toolkit: The Mathematics of Black-Hole Mechanics* (Cambridge University Press, Cambridge, 2004)
51. E. Poisson, W. Israel, Phys. Rev. D **41**, 1796 (1990)
52. D. Psaltis, D. Perrodin, K. R. Dienes and I. Mocioiu, Phys. Rev. Lett. **100**, 091101 (2008) [Erratum: Phys. Rev. Lett. **100**, 119902 (2008)] [arXiv:0710.4564](#) [astro-ph]
53. D.C. Robinson, Phys. Rev. Lett. **34**, 905 (1975)
54. T.P. Sotiriou, V. Faraoni, Phys. Rev. Lett. **108**, 081103 (2012), [arXiv:1109.6324](#) [gr-qc]
55. J. Thornburg, Living Rev. Rel. **10**, 3 (2007), [arXiv:gr-qc/0512169](#)
56. R.C. Tolman, Proc. Nat. Acad. Sci. **20**, 169 (1934) [Gen. Rel. Grav. **29**, 935 (1997)]
57. P.K. Townsend, [arXiv:gr-qc/9707012](#)
58. M.S. Volkov, D.V. Galtsov, JETP Lett. **50**, 346 (1989) [Pisma Zh. Eksp. Teor. Fiz. **50**, 312 (1989)]
59. M.S. Volkov, D.V. Gal'tsov, Phys. Rept. **319**, 1 (1999), [arXiv:hep-th/9810070](#)
60. R.M. Wald, *General Relativity* (University of Chicago Press, Chicago, 1984)
61. R.M. Wald, V. Iyer, Phys. Rev. D **44**, 3719 (1991)
62. M. Walker, J. Math. Phys. **11**, 2280 (1970)
63. B. Waugh, K. Lake, Phys. Rev. D **38**, 1315 (1988)
64. K. Yagi, N. Yunes and T. Tanaka, Phys. Rev. D **86**, 044037 (2012) [Phys. Rev. D **89**, 049902 (2014)] [arXiv:1206.6130](#) [gr-qc]
65. N. Yunes, F. Pretorius, Phys. Rev. D **79**, 084043 (2009), [arXiv:0902.4669](#) [gr-qc]
66. S.N. Zhang, Int. J. Mod. Phys. D **20**, 1891 (2011), [arXiv:1003.1359](#) [gr-qc]
67. Y. Zhang, Y. Zhu, L. Modesto, C. Bambi, Eur. Phys. J. C **75**, 96 (2015), [arXiv:1404.4770](#) [gr-qc]

<http://www.springer.com/978-981-10-4523-3>

Black Holes: A Laboratory for Testing Strong Gravity

Bambi, C.

2017, XV, 340 p. 123 illus., 117 illus. in color.,

Hardcover

ISBN: 978-981-10-4523-3